IEEE Access
Multidisciplinary ⋮ Rapid Review ⋮ Open Access Journal

Received October 30, 2020, accepted November 15, 2020, date of publication November 24, 2020,
date of current version December 7, 2020.

Digital Object Identifier 10.1109/ACCESS.2020.3039877

New Fault-Location Algorithm for Series-Compensated Double-Circuit Transmission Line

DAIYING CAI AND JUN ZHANG
Chongqing Key Laboratory of Complex Systems and Bionic Control, Chongqing University of Posts and Telecommunications, Chongqing 400065, China
Smart Energy Research Center, Chongqing University of Posts and Telecommunications, Chongqing 400065, China

Corresponding author: Daiying Cai (18725938931@163.com)

This work was supported in part by the National Natural Science Foundation Project of China under Grant 61703066, in part by the Natural Science Foundation Project of Chongqing under Grant cstc2018jcyjAX0536, and in part by the Chongqing Technology Innovation and Application Development Project under Grant cstc2019jscx-fxydX0042 and Grant cstc2019jscx-zdztzxX0053.

ABSTRACT This paper proposes a new fault location algorithm to accurately locate the faults of series-compensated double-circuit transmission line and improve the stability of power system operation, which is not affected by fault types. The proposed algorithm is based on asynchronous voltage and current at both ends of the line, the pre-fault voltage and current are used to synchronize time. The six-sequence component transformation is introduced, and with the help of the phase-sequence selection rule, the proposed algorithm eliminates the non-linear impedance of metal oxide varistor (MOV). Simultaneously, to confirm the robustness of the algorithm, different fault types, different fault initial angles and different fault resistances are taken into account in the system simulation. Not only that, the influence of series capacitors (SCs) installation positions, line parameter errors, different sampling rates and measurement errors are also tested. In general, the proposed fault-location algorithm has excellent performance. PSCAD/EMTDC and MATLAB are used in simulation studies, the results show that the maximum estimated error of fault-location does not exceed 1.8631%.

INDEX TERMS Keyword series-compensated double-circuit transmission line, fault-location, six-sequence component transformation, metal oxide varistor (MOV), series capacitors (SCs).

I. INTRODUCTION

Continuous and reliable power supply is the goal of power system operation. However, faults in the power system are unavoidable. Transmission lines are the most fault-prone part of the power system [1]. Fault-location is very important to the economic operation of the power system and the quality of power supply. The form of the fault is a short circuit between conductors or to ground. The fault locator is used to accurately locate the fault of the transmission line, it can reduce the maintenance time, thereby improving the availability of the system.

To determine the faulted location of transmission lines, several fault-location algorithms are proposed [2]–[12]. These algorithms can be divided into two categories. In the first category, single-terminal voltage and current are used in fault-location algorithm [2]–[6]. In these algorithms, it may be difficult to accurately determine the locations of the faults, since these algorithms are usually valid under approximate assumptions, in the absence of data from the other terminal, existing algorithms generally have accuracy problems. For another category algorithm, two-terminal voltage and current are employed [7]–[12]. In the latter category, phasor measurement units (PMUs) are adopted to measure voltage and current [7]–[11], asynchronous voltage and current are used in [9], [12].

SCs are widely used in long-distance transmission line to improve power transmission capabilities [13]. It also incre-ases the margin of transient stability, optimizes the load distribution of parallel transmission line, and reduces system losses.

The protector of SC device is usually integrated together to provide overcurrent protection, as shown in Figure 1, SC consists of series capacitor branch, MOV protection branch, gap protection branch and protection controller [14]. Line faults are accompanied by tremendous currents, the protection controller will trigger MOV-protection or gap-protection through current-threshold, then the current will decrease. If current is lower than conduction threshold of series capacitor, the series capacitor reconducts. Generally, MOV provides first

The associate editor coordinating the review of this manuscript and approving it for publication was Youqing Wang.

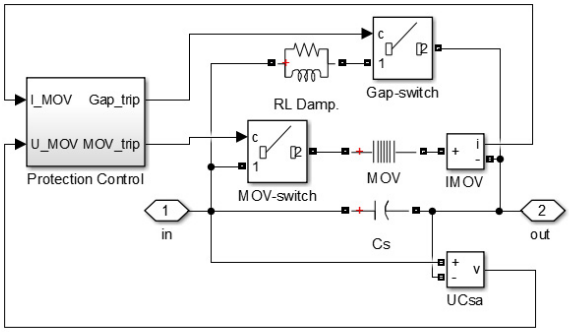

FIGURE 1. Series Capacitor device.

protection and gap provides secondary protection because of the conduction threshold of MOV is lower than gap. When line fault happens, internal series capacitor, MOV and gap alternately conduct in each fundam-ental frequency cycle [14]. The on-off time of each branch of each fundamental frequency period depends on the fault current. It means that the behavior of the impedances of SCs device at fault phases are highly non-linear, which is in contrast to the linear impedances of conventional lines. Therefore, developing fault location algorithm specially for series-compensated line is indispensable.

In recent years, fault-location of series-compensated line has become a research focus [15]–[24]. Several fault-location algorithms of single-circuit series-compensated transmission line were proposed [15]–[21], and the fault-location of double-circuit series-compensated line was studied in [22]–[24]. In [15], [17], the impedance of the MOV is estimated through the impedance characteristic curve, and then the fault distance is estimated. In [16], transmission line between the fault point and the installation point of the SCs is regarded as RLC series circuit, and the fault-location algorithm is obtained. SCs device with MOV protection and gap protection are applied in [18], [21], MOVs are bypassed by gap protection in the later stage of faults, then the influence of MOVs on fault-location is eliminated. The symmetrical component method is employed in [19], an impedance-based algorithm for single-circuit transmission line is proposed, the impedances of MOVs are eliminated. Since the double-circuit transm-ission line is more complicated in structure than the single- circuit transmission line, the traditional symmetrical component method cannot directly decouple the double-circuit transmission line, and the algorithm of [19] is not suitable for symmetrical faults. In [20], assuming that voltages at two bus are equal, a single-phase fault location method is proposed. In [22], the six-sequence component method is employed to calculate the fault distance. In [23], the zero-sequence equivalent network of double-circuit transmission line is established to estimate the fault distance. A specific phase-to-mode transformation is introduced in [24], and a pi-model of transmission line is established to obtain the fault distance.

This paper presents a new fault location algorithm for series-compensated double-circuit transmission line, which is not affected by fault types. Asynchronous voltage and current at both terminals of the lines are used to estimate the fault distance. The pre-fault voltage and current at both terminals are used for time synchronization, and the six-sequence component method is introduced to convert the voltage and current into the mode domain, the proposed fault-location algorithm eliminates nonlinear impedances generated by MOVs, and it is suitable for all fault types including fault between different circuits.

The rest of this paper is organized as follows. The second section explains the basic principles of series-compensated double-circuit line and derives the fault-location algorithm. In the third section, the results of PSCAD and MATLAB are given to verify the proposed algorithm performance. The fourth part summarizes this paper.

The notations adopted in this paper are summarized first.

M, N	Two terminals of the series-compensated transmission line.
L, R	Two terminals of the SCs device
i	Six-component index, $i = 1, 2, 3, 4, 5, 6$ respectively.
Z_c, γ	line characteristic impedance and line propagation constant, respectively.
l	length of series-compensated transmission line.
l_c	SCs device away from M-terminal distance
x	Fault point away from M-terminal distance
R_f	fault transition resistance
I_{M-pre}, U_{M-pre}	pre-fault current and voltage at the M-terminal, respectively.
I_{N-pre}, U_{N-pre}	pre-fault current and voltage at the N-terminal, respectively.
I_{L-pre}, I_{R-pre}	pre-fault current at the point L and point R, respectively.
Z_{ci}, γ_i	i_{th} sequence characteristic impedance and line propagation constant, respectively.
I_{Ms}, U_{Ms}	sequence current and sequence voltage at the M-terminal, respectively.
I_{Ns}, U_{Ns}	sequence current and sequence voltage at the N-terminal, respectively.
I_{Msi}, U_{Msi}	i_{th} sequence current and sequence voltage at the M-terminal, respectively.
I_{Nsi}, U_{Nsi}	voltage at the N-terminal, respectively.
I_{Mfs}, I_{Nfs}	sequence current of both sides of the fault point, respectively.
I_{fs}, U_{fs}	sequence current and sequence voltage at the fault point, respectively.
I_{SC1s}, I_{SC2s}	i_{th} sequence current and sequence sequence current of both sides of the SCs device, respectively.
I_{SC1si}	i_{th} sequence current of left side of SCs device
I_{SC2si}	i_{th} sequence current of right side of SCs device
ΔV_{SCsi}	i_{th} sequence voltage-drop of SCs device
$[Z_{SC}]$	impedance matrix of SCs device
$[Z_{SCs}]$	sequence impedance matrix of SCs device

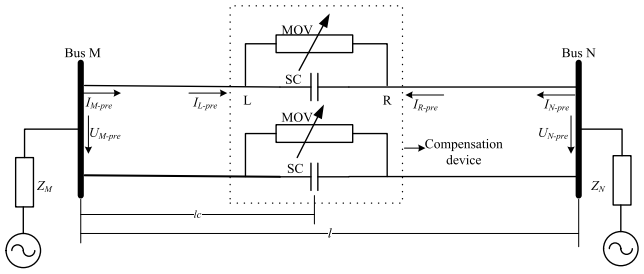

FIGURE 2. Series-compensated double-circuit transmission line.

II. PROPOSED THE FAULT LOCATION ALGORITHM

The schematic diagram of a series-compensated double-circuit transmission line is shown in Figure 2. The distributed parameter line model is adopted. MOVs connected in parallel with SCs to provide over voltage protection. MOV has nonlinear VI-characteristics.

There are mutual electromagnetic effects between circuits and phases in double-circuit transmission lines, and SCs device are installed on double-circuit line, except for the SCs device, the remaining line is considered to be evenly transposed. Under this basis, the six-sequence component method can be used to decouple the line.

In the six-sequence component method, firstly, the common-component and the differential-component are used to eliminate the mutual impedances between circuits [8]. And then, the mutual impedances between the phases are eliminated by the symmetrical component method. The deviation is carried out with reference to [25]. Based on the conclusion of [25], the transformation matrix $[Q]$ is used to decouple the voltage and current, resulting in the following six-sequence network of the distributed parameter model. The voltage and current of the transmission network can be written as six-sequence components, and the formula is as follows:

$$[Q] = \frac{1}{3}\begin{bmatrix} 1 & a & a^2 & 1 & a & a^2 \\ 1 & a^2 & a & 1 & a^2 & a \\ 1 & 1 & 1 & 1 & 1 & 1 \\ 1 & a & a^2 & -1 & -a & -a^2 \\ 1 & a^2 & a & -1 & -a^2 & -a \\ 1 & 1 & 1 & -1 & -1 & -1 \end{bmatrix} \quad (1)$$

$$[I_S] = [Q][I] \quad (2)$$

$$[U_S] = [Q][U] \quad (3)$$

where $a = e^{j120}$.

$$[I_S] = \begin{bmatrix} I_{T1} & I_{T2} & I_{T0} & I_{F1} & I_{F2} & I_{F0} \end{bmatrix}^{\mathrm{T}} \quad (4)$$

$$[U_S] = \begin{bmatrix} U_{T1} & U_{T2} & U_{T0} & U_{F1} & U_{F2} & U_{F0} \end{bmatrix}^{\mathrm{T}} \quad (5)$$

I and U refer to the current and voltage in the phase domain, I_S and U_S refer to sequence current and voltage. The indexes T and F represent the common-component circuit and the differential-component circuit, respectively, and the two independent circuits with the same and reverse current direction as the original current, the indexes 1, 2 and 0 represent the positive, negative and zero sequence components.

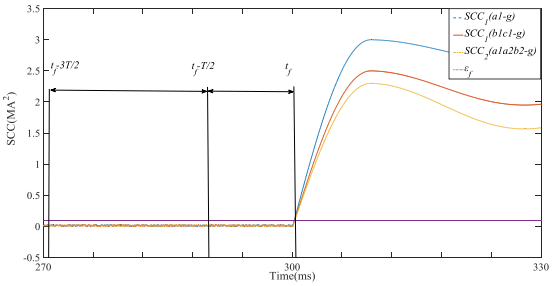

FIGURE 3. Curve of SCC and time window.

A. DATA SYNCHRONIZATION

This paper uses the pre-fault voltage and current measured at both terminals to synchronize phase. If the pre-fault synchronization scheme is adopted, SC device can be regarded as constant capacitance, so the difficulty of calculating δ are greatly reduced. At the same time, in order to obtain accurate pre-fault voltage and current, it is necessary to accurately determine the trigger time of fault. The method of detecting faults is introduced [26], SCC_j is defined as follow:

$$SCC_j = I_{aj}^2 + I_{bj}^2 + I_{cj}^2 \quad (6)$$

j ($j = 1, 2$) represents the circuit number, I_{aj}, I_{bj} and I_{cj} refers to the three-phase current of circuit j measured at bus M, respectively.

Obviously, when there is no fault, I_{aj}, I_{bj} and I_{cj} have the same amplitude and the phase angles difference of 120°. Once a fault occurs, SCC_j will be greater than zero. a threshold ($\varepsilon_f = 0.1$) is set to detect faults, and the detection effect is given in the Figure 3. As shown in Figure 3, the sampling time window is $[t_f - 3T/2, t_f - T/2]$, t_f is fault trigger time, T is the three-phase period.

Refer to the double-circuit transmission line shown in Figure 2, after obtaining the pre-fault voltage and current at M-terminal, assuming that the M-terminal is the synchronization reference point, the current at point L is calculated as follows:

$$I_{L-pre} = \frac{-1}{Z_c}\sinh(\gamma l_c)U_{M-pre} + \cosh(\gamma l_c)I_{M-pre} \quad (7)$$

I_{L-pre} refers to the pre-fault current at point L, U_{M-pre} and I_{M-pre} refer to the voltage and current of the pre-fault bus M, respectively.

Due to there is a synchronous measurement error at both ends, if the phasor phase at bus M is used as a reference, the voltage and current measured by the bus N need to be corrected by the synchronization Angle, which is assumed to be δ. At this point, the corrected current at N can be obtained.

$$I_{R-pre} = e^{j\delta} \cdot (-\frac{1}{Z_c}\sinh(\gamma(l - l_c))U_{N-pre} + \cosh(\gamma(l - l_c))I_{N-pre}) \quad (8)$$

I_{R-pre} refers to the pre-fault corrected current at point R, U_{N-pre} and I_{N-pre} refer to the voltage and current of the pre-fault bus N, respectively.

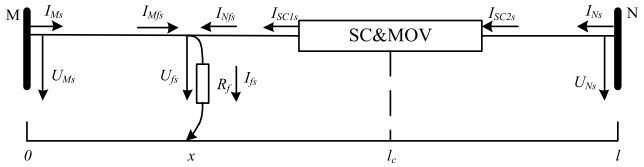

FIGURE 4. Six-sequence network for series-compensated double-circuit transmission line for a fault on the left side of the SC & MOV device.

Obviously, since SC devices are pure capacitors at this time, the currents at both terminals of the SC device are equal.

$$I_{L-pre} = -I_{R-pre} \tag{9}$$

The synchronization angle δ can be derived from the Eq (10):

$$\delta = \arccos(Re \cdot (\frac{-K_1}{K_2})) \tag{10}$$

where Re·() represents the real part, K_1 and K_2 are as follows:

$$K_1 = \cosh(\gamma l_c) I_{M-pre} Z_c - \sinh(\gamma l_c) U_{M-pre} \tag{11}$$

$$K_2 = -\cosh(\gamma(l - l_c)) I_{N-pre} Z_c + \sinh(\gamma(l - l_c)) U_{N-pre} \tag{12}$$

It should be noted that, to simplify the process of derivation, the voltage and current at the M-terminal and N-terminal are synchronized in the derivation below.

B. FAULT LOCATION METHOD

1) SUBROUTINE I: FAULT ON THE LEFT SIDE OF THE SERIES COMPENSATOR

The equivalent six-sequence circuit with the fault on the left side of SCs device is shown in Figure 4. Now, the fault distance x can be obtained by the i_{th} sequence measurements and parameters of the transmission line [27]. The fault distance x satisfies the Eq (13), ΔV_{SCsi} is i_{th} sequence voltage dropped across SCs from Node N to Node M.

$$x = \tanh^{-1}(\frac{-B_i + \Delta V_{SCsi}}{A_i})/\gamma_i \tag{13}$$

where

$$A_i = Z_{ci}\cosh(\gamma_i l_c) I_{Msi} - \sinh(\gamma_i l_c) U_{Msi} + Z_{ci} I_{SC1si} \tag{14}$$

$$B_i = \cosh(\gamma_i l_c) U_{Msi} - Z_{ci}\sinh(\gamma_i l_c) I_{Msi} - U_{SC2si} \tag{15}$$

In above (14) and (15), U_{SCs2} can be obtained by (16). I_{SC1si} and I_{SC2si} are sequence current at both sides of the SCs, and they are equal, can be derive from bus N.

$$U_{SC2si} = \cosh(\gamma_i(l - l_c) U_{Nsi} - Z_{ci}\sinh(\gamma_i(l - l_c)) I_{Nsi} \tag{16}$$

$$I_{SC1si} = I_{SC2si} = \frac{-1}{Z_{ci}}\sinh(\gamma_i(l - l_c)) U_{Nsi} + \cosh(\gamma_i(l - l_c)) I_{Nsi} \tag{17}$$

In (13), there are ΔV_{SCsi} and x two unknown variables, so determine ΔV_{SCsi} is main problem of fault-location. However, MOV is a nonlinear impedance component, the estimation of ΔV_{SCsi} is not straightforward. In order to overcome this limitation, the fault-location equation (13) is rearranged as:

$$A_i \tanh(\gamma_i x) + B_i + \Delta V_{SCsi} = 0 \tag{18}$$

From the circuit shown in Figure 4, the sequence voltage drop of the SCs device satisfies (19). In (19), Z_{SCs} is obtained by the (20).

$$[\Delta V_{SCsi}] = [Z_{SCs}]\,[I_{SC2si}] \tag{19}$$

$$[Z_{SCs}] = \left[Q^{-1}\right][Z_{SC}]\,[Q] \tag{20}$$

where

$$[\Delta V_{SCsi}] = [\Delta V_{SCs1}, \Delta V_{SCs2}, \Delta V_{SCs3}, \Delta V_{SCs4}, \Delta V_{SCs5}, \Delta V_{SCs6}]^T \tag{21}$$

$$[I_{SC2si}] = [I_{SC2s1}, I_{SC2s2}, I_{SC2s3}, I_{SC2s4}, I_{SC2s5}, I_{SC2s6}]^T \tag{22}$$

In phase domain, the impedance matrix of the SC&MOV device is as follows:

$$[Z_{SC}] = \begin{bmatrix} Z_{a1} & & & & & \\ & Z_{b1} & & & & \\ & & Z_{c1} & & & \\ & & & Z_{a2} & & \\ & & & & Z_{b2} & \\ & & & & & Z_{c2} \end{bmatrix} \tag{23}$$

Z_{a1}, Z_{b1}, Z_{c1}, Z_{a2}, Z_{b2} and Z_{c2} refer to impedances of SC&MOV device in each line. $[Z_{SCs}]$ can be obtained through (20), which is shown in the Appendix.

Bring $[Z_{SCs}]$ into (19), and then sum all sequence components of $[\Delta V_{SCsi}]$, and (24) is derived, where only Z_{a1} still exists.

$$\sum_i^6 V_{SCsi} = Z_{a1}(\sum_i^6 I_{SC2si}) \tag{24}$$

Assuming that the impedance of the SC in healthy line and faulted line is Z_{Cap} and Z_M, respectively. Z_{Cap} is a constant capacitance, Z_M is indefinite impedance. To eliminated the impedance Z_M, Z_{a1} cannot be equal to Z_M in (24), in another word, phase a1 cannot be a fault phase, and the phase-sequence ($a1$, $b1$, $c1$, $a2$, $b2$, $c2$) of the three-phase system is artificially selected [27], the proper phase-sequence is necessary. The process shown in Figure 6, for example, assuming the fault type is $a1a2$ -g, after selecting the phase sequence according to (25), the fault type is converted to $b1b2$-g.

$$(a1, a2) \rightarrow (b1, b2) \rightarrow (c1, c2) \rightarrow (a1, a2) \rightarrow \ldots \tag{25}$$

Similarly, summing all the sequence components in (18), the fault locating function $f\ (x)$ is obtained, which is shown in (26).

$$f(x) = \sum_i^6 A_i \tanh(\gamma_i x) + \sum_i^6 B_i + Z_{a1}(\sum_i^6 I_{SC2si}) \tag{26}$$

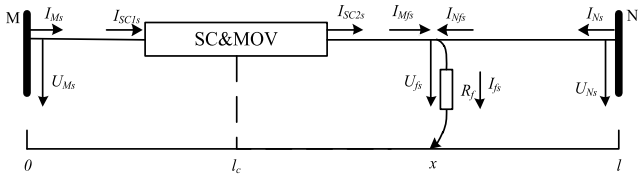

FIGURE 5. Six-sequence network for series-compensated double-circuit transmission line for a fault on the right side of the SC & MOV device.

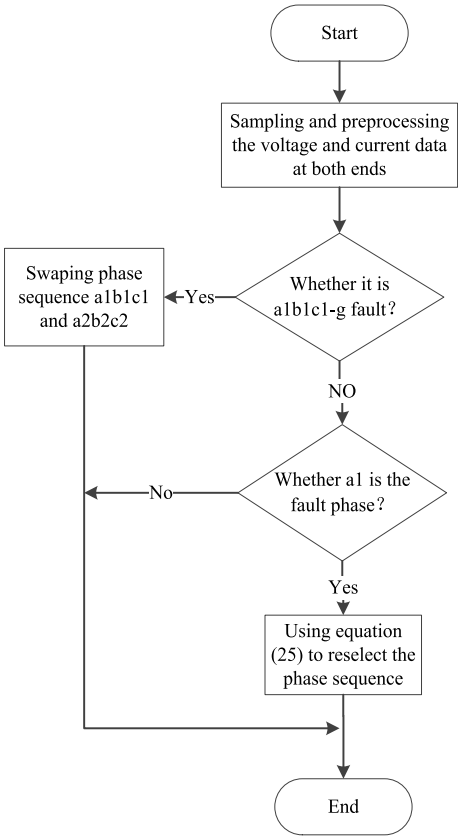

FIGURE 6. Phase-sequence reselection flowchart.

2) SUBROUTINE II: FAULT ON THE RIGHT SIDE OF THE SERIES COMPENSATOR

The equivalent six-sequence circuit of the fault on the right side of SCs is shown in Figure 5. The derivation process is similar to subroutine I, and the fault distance estimation equation is given in (27).

$$f(x) = \sum_{i}^{6} C_i \tanh(\gamma_i(l-x)) + \sum_{i}^{6} D_i + Z_{a1}\left(\sum_{i}^{6} I_{SC1si}\right) \quad (27)$$

$$C_i = Z_{ci}\cosh(\gamma_i(l-l_c))I_{Nsi} - \sinh(\gamma_i(l-l_c))U_{Nsi} + Z_{ci}I_{SC2i} \quad (28)$$

$$D_i = \cosh(\gamma_i(l-l_c))U_{Nsi} - Z_{ci}\sinh(\gamma_i(l-l_c))I_{Nsi} - U_{SC1i} \quad (29)$$

$$U_{SC1si} = \cosh(\gamma_i l_c)U_{Msi} - Z_{ci}\sinh(\gamma_i l_c)I_{Msi} \quad (30)$$

$$I_{SC1si} = I_{SC2si} = \frac{-1}{Z_{ci}}\sinh(\gamma_i l_c)U_{Msi} + \cosh(\gamma_i l_c)I_{Msi} \quad (31)$$

ΔV_{SCsi} is sequence voltage dropped across SCs device from Node M to Node N.

Due to the possibility of pseudo roots when solving $f(x)$, in order to solve the problem of pseudo roots. Bringing (26) or (27) into (32), the possible value of x can be obtained. Obviously, the solution of $f(x)$ is a complex number, and only the solution that satisfies its real part and imaginary part equal to 0 is meaningful. In other words, x satisfies (33) is the true estimated fault distance, and $\varepsilon(\varepsilon = 25)$ is an empirical value, and the value of ε is derived from subsequent experiments.

$$\mathrm{Re}\cdot(f(x)) = 0 \quad (32)$$

$$|\mathrm{Im}\cdot(f(x))| \leq \varepsilon \quad (33)$$

According to the algorithm proposed in the above sections, subroutine I and subroutine II are applicable to the fault location on the left and right sides of the SCs device, respectively. Therefore, it is crucial to determine the fault section. Obviously, the reasonable solution x of subroutine I and subroutine II satisfy the boundary cond-itions [0, lc] and [lc, l], respectively. First input the data into subroutine I to calculate the fault distance x, if x meets the boundary conditions [0, lc], it can be determined that the fault is located on the left side of the SCs device; on the contrary, the fault is located on the right side of the SCs device, and then input data to subroutine II, and the fault distance x is calculated by (27), and x must meet the boundary condition [lc, l].

C. CALCULATION PROCESS

The flowchart of the proposed fault location method is shown in Figure 7. According to the proposed algorithm in the previous article, the fault-location process is as follows:

Step 1: Recording and sampling the voltage and current of the both ends of the line. Eq (10) is used for time synchro-nization at both ends;

Step 2: Using (6) to determine the fault phases, if phase a1 is fault phase, reselect the phase sequence by progress shown in Figure 6;

Step 3: Using (2) and (3) to decouple the data obtained by step 1;

Step 4: Input data obtained by step 3 into subroutine I to obtain the fault distance x, if x meets the boundary condition of subroutine I [0, lc], skip to step 6;

Step 5: Input data obtained by step 3 into subroutine II to obtain the fault distance x. If x meets the boundary condition of subroutine II [lc, l], skip to step 6.

Step 6: Bring the x obtained by step 4 or step 5 into (33) to eliminate the possibility of pseudo-roots. If x is less than the threshold ε, output x as the fault distance.

III. ALGORITHM PERFORMANCE ANALYSIS

A. TEST SYSTEM

This section presents the evaluation of the proposed fault location method. PSCAD/EMTDC is used to simulate series-compensated double-circuit line under different fault conditions. MATLAB will read the simulation results and estimates the location of each fault. Figure 2 shows a 315 kV, 300 km, 50 Hz double-circuit transmission line compensated at the degree of 40%($C = 29.11\mu$F) is simulated, the SCs device

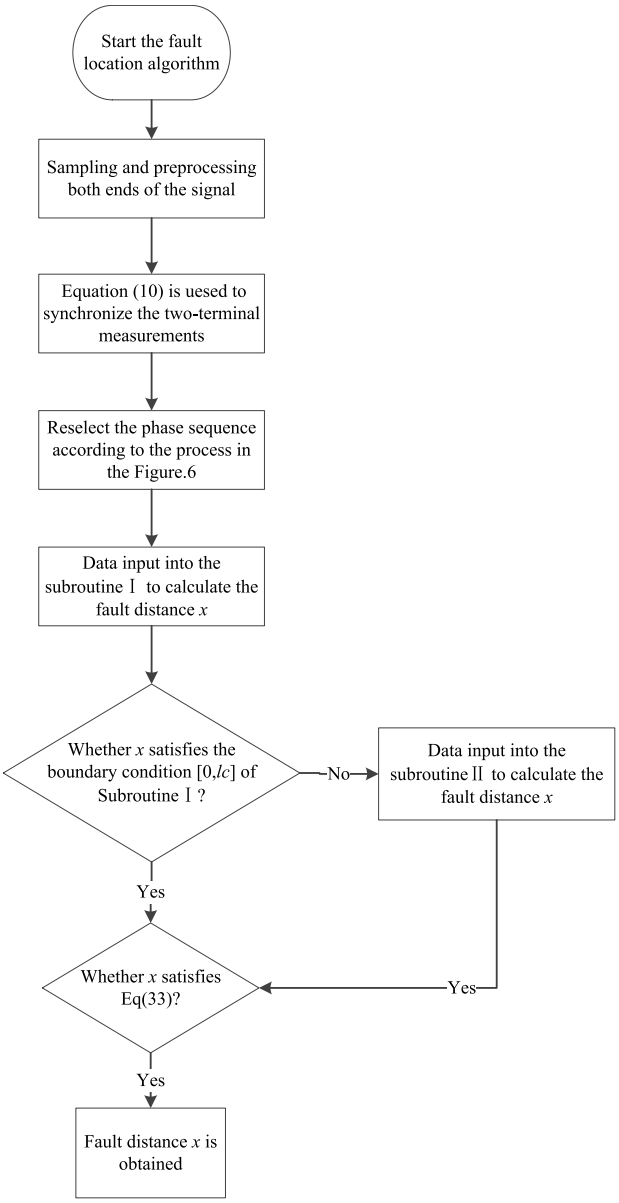

FIGURE 7. Flowchart of fault-location algorithm.

is installed 150 km away from the terminal-M [28]. The voltage sources parameters and transmission line parameters are shown in Table.1 and Table.2, respectively. Regardless of the influence of meters and transformers, current and voltage transformers are considered as ideal equipment. Since the proposed algorithm only uses the series capacitances in the SCs device, the type and model of SCs device has no influence on the algorithm. However, the model of MOV is similar to [16], [19], [22], [24]. The correlation error is adopted as follows:

$$\text{Error}(\%) = \frac{|\text{estimated length - actual length}|}{\text{line branch length}} \quad (34)$$

B. SYNCHRONIZE EFFORTS

The phase distribution curve of different SCs device installation positions is shown in Figure 8. θ represents the voltage phase distribution curve of the voltage recorded on the remote terminal (bus N). δ is the phase error distribution curve, θ_c is the phase distribution curve after corrected, and θ_i is the phase distribution curve of the ideal synchronization voltage. It can be clearly seen that the curves θ_i and θ_c are always very close, indicating that the synchronization effect is excellent.

TABLE 1. Voltage source data.

Quantity	Source M	Source N
Ermf (KV)	$315\angle 0^\circ$	$300\angle 10^\circ$
Pos. Seq. Impedance (Ω)	1.125 + j15.773	1.042 + j14.110
Zero. Seq. Impedance (Ω)	6.421 + j39.562	5.447 + j35.54

TABLE 2. Transmission line data.

Parameter	Self	Mutl-Pha.	Mutl-Cir.
R (Ω/km)	0.0880	0.0611	0.0611
L (mH/km)	0.0019	0.0009	0.0008
C (nF/km)	$1.0106e^{-8}$	$-1.5554e^{-9}$	$-7.0293e^{-10}$

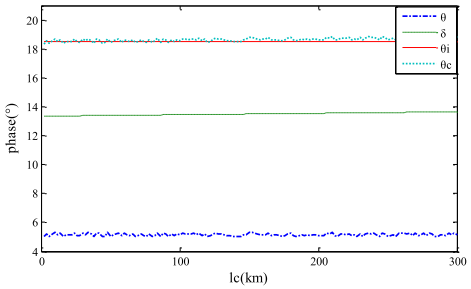

FIGURE 8. Synchronize efforts of different SCs location.

TABLE 3. Results of simulation cases.

Erea	Type	x(km)	R_f(Ω)	Angle(°)	Sub-Ⅰ	Sub-Ⅱ	Error(%)
Left	b1-g	31	10	135	31.05	-5744	0.0155
	a2-g	85	10	45	84.59	-7355	0.1359
	c1a2-g	69	100	90	68.58	7920	0.1396
	a2c2-g	61	100	45	61.19	-3205	0.0639
	a1b1	113	0.1	90	114.6	-316	0.5424
	a1a2	117	100	45	117.7	8443	0.2463
	b1b2c2-g	62	0.1	90	62.02	-4092	0.0050
	a1b1b2-g	146	100	45	146.3	1186	0.1254
Right	a1-g	172	0.1	90	-7045	171.25	0.2515
	b1-g	235	100	45	-5440	234.10	0.2999
	a1c1-g	159	100	45	1279	159.23	0.0779
	a2b2-g	214	10	135	5369	215.42	0.4746
	a1a2	164	100	45	-7144	166.32	0.7726
	b1c2	278	10	45	8649	278.86	0.2877
	b1c1b2-g	179	100	90	9454	179.69	0.2316
	c1b2c2-g	261	0.1	90	2142	261.79	0.2648

C. RESULTS OF TEST CASES

Table.3 shows the effect of the proposed fault location algorithm. In Table 1, tests are carried out for different fault resistances, different fault angles and different fault types.

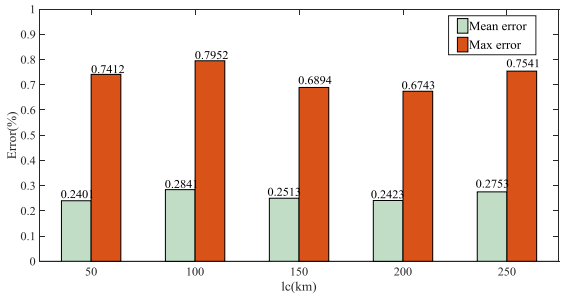

FIGURE 9. Mean and max error considering different *lc*.

In the cases of faults locate in the left side of the SCs device, all results of subroutine I satisfy the interval [0, l_c], and all results of subroutine II does not satisfy the interval [l_c, l], so these faults are determined in left side of SCs device. In the fault cases of the right side of the SCs device, the results of subroutine I are not in the interval [0, l_c], and all results of subroutine II in the interval [l_c, l], so these faults are determined in right side of SCs device.

At the same time, in Figure 10, $|\mathrm{Im}(f(x))|$ corresponds to different fault types and locations are less than the threshold ε ($\varepsilon = 25$), indicating that there is no possibility of pseudo roots.

D. INFLUENCE OF SCs INSTALLATION POSITION

The influence of the different SCs device installation locations is shown in Figure 9. Five different l_c values (50,100,150,200 and 250 km) are adopted, the other fault conditions are the same as Table 3. In Figure 9, the maximum value of the mean error is 0.2753%, the maximum value of the max error is 0.7952%. Moreover, the fluctuation of error is very small, so the accuracy can be accepted in different SCs installation positions.

E. COMPARED TO PREVIOUS ALGORITHMS

In order to prove the superiority in the proposed algorithm in this paper, it was compared with the previous algorithms in [16] and [19]. The results are shown in Table 4. The fault conditions are the same as in Table 3. It is worth noting that the algorithm in [19] is only applicable to single-circuit transmission line. Therefore, assume that the mutual inductance between the circuits is zero. Since the algorithm in [19] only focuses on asymmetric faults, Table 4 only lists the location results of asymmetric faults.

In Table 4, the maximum error of the proposed algorithm in this paper is 0.7726%, the maximum error of the proposed algorithm in [16] is 2.1281%, and the maximum error of the proposed algorithm in [19] is 16.38%. It can be explained as follows: in [16], RLC circuit is used to replace the transm-ission line from the SCs device to the fault point, which will inevitably produce additional errors; in [19], the mutual inductance of different transmission line circuits is ignored, the results of Table 4 indicate that the mutual inductance between circuits is essential to locate fault, so the algorithm in [19] cannot be applied to double-circuit series compen-sation transmission line. The results in Table 4 show

TABLE 4. Results of different algorithm.

Fault types	Actual fault distance(p.u.)	Proposed algorithm(%)	Algorithm in [16](%)	Algorithm in [19](%)
b1-g	0.1033	0.0155	1.8881	14.16
a2-g	0.2833	0.1359	1.1945	12.23
a1-g	0.5733	0.2515	0.3204	6.481
b1-g	0.7833	0.2999	1.1945	7.234
c1a2-g	0.2300	0.1396	2.1281	14.56
a2c2-g	0.2033	0.0639	1.2641	12.92
a1c1-g	0.5300	0.0779	0.4801	10.08
a2b2-g	0.7133	0.4746	1.1816	14.10
a1b1	0.3767	0.5424	0.6089	11.37
a1a2	0.3900	0.2463	0.5809	7.091
a1a2	0.5467	0.7726	0.4916	10.20
b1c2	0.9267	0.2877	2.1104	16.38
b1b2c2-g	0.2067	0.005	1.1464	-
a1b1b2-g	0.4867	0.1254	0.3736	-
b1c1b2-g	0.5967	0.2316	0.73561	-
c1b2c2-g	0.8700	0.2648	1.5041	-

that the algorithm proposed in this paper is more accurate. Not only that, the algorithm proposed in this paper has a unified fault location formula for all fault types, while the algorithm of [19] has different fault location formulas for single-phase faults and two-phase faults. The algorithm of [19] requires additional fault diagnosis before fault location.

F. EFFECT OF ERROR IN TRANSMISSION LINE PARAMETERS

In the actual transmission line, the line parameters cannot be completely accurate. Therefore, to verify the performance of the proposed fault location algorithm under different line parameter errors is necessary.

In Figure 11, 1%, 2% and 3% parameter errors are considered, the other fault conditions are the same as Table 3. The mean error and max error are shown in Figure 10, when 3% parameter error is adopted, the mean error and the max error reach the maximums, which are 1.0965% and 1.7874%, respectively. As expected, the fault location accuracy is affected by transmission line parameter errors, however, from a practical perspective, the accuracy under parameter error is still acceptable.

G. INFLUENCE OF MEASUREMENT ERRORS AND DIFFERENT SAMPLING RATES

In order to test the influence of the measurement errors, according to the IEEE standard [30], 3% measurement error is considered. The mean error and max error for different fault types are shown in Figure.12. The fault conditions are the same as Tables 3. Tables 3 and Figure 12 shows that the max error increased from 0.7726% to 1.8631%. It can be seen that the fault location accuracy is affected by themeasurement error. However, the accuracy is still acceptable in practice.

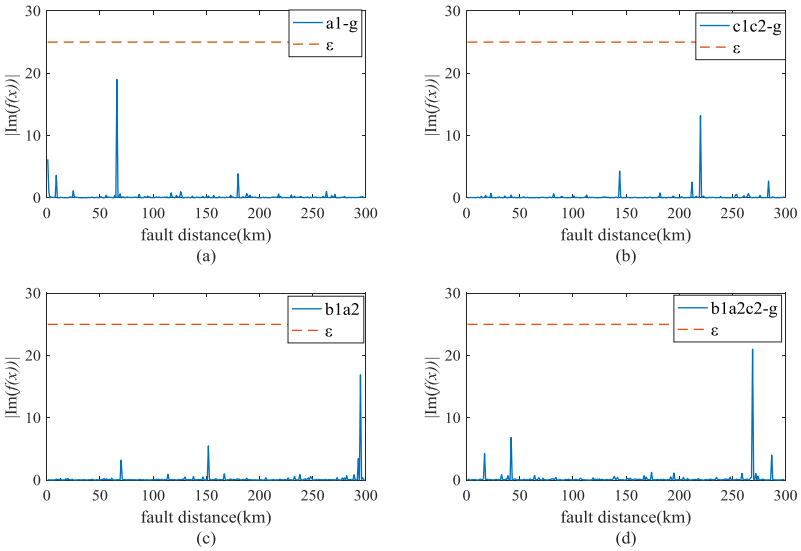

FIGURE 10. Different fault distance distribution curves of |Im(f(x))|. (a) a1-g fault curve (b) c1c2-g fault curve (c) b1a2-g fault curve (d) b1a2c2-g fault curve.

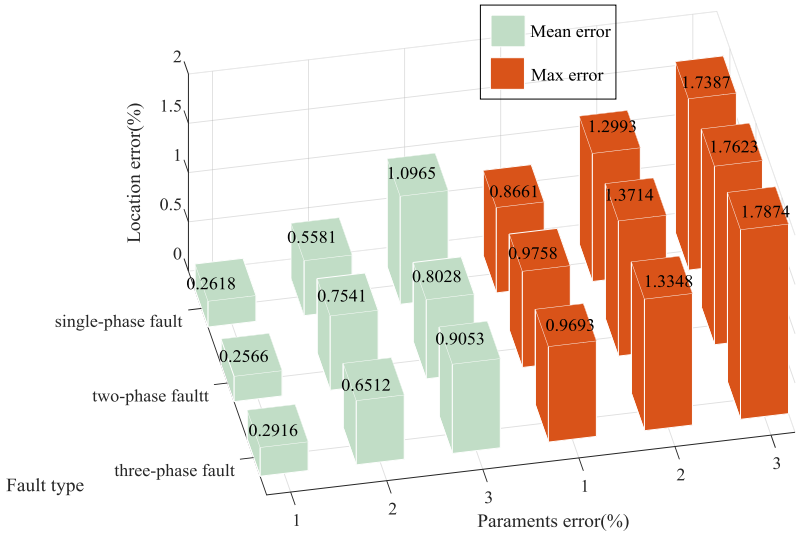

FIGURE 11. Mean and max error considering transmission lines parameters errors.

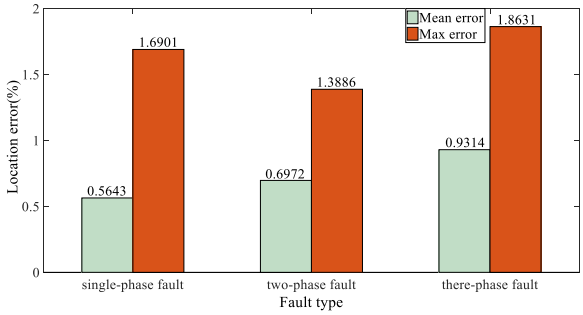

FIGURE 12. Mean and max error in fault location considering measurement errors.

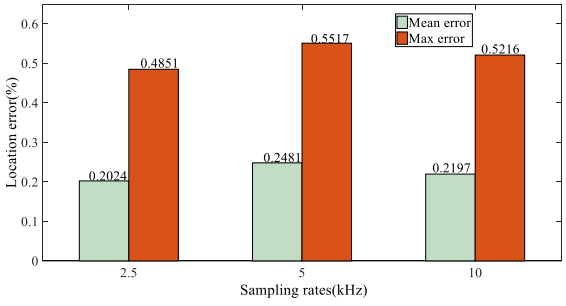

FIGURE 13. Mean and max error considering different sampling rates.

In addition, the results of new algorithm using different sampling rates (2.5, 5 and 10 kHz) are shown in Figure 13, it's easy to see changing the sampling rates has little effect on accuracy. As a result, it can be concluded that the proposed algorithm suitable for different sampling rates.

IV. CONCLUSION

This paper presents a fault location algorithm for series-compensated double-circuit transmission line. The proposed algorithm is based on asynchronous voltage and current at both ends of the line, the pre-fault voltage and current

$$[Z_{SCs}] = \frac{1}{6}\begin{bmatrix} Z_{a1}+Z_{b1}+Z_{c1}+Z_{a2}+Z_{b2}+Z_{c2} & Z_{a1}+a^2Z_{b1}+aZ_{c1}+Z_{a2}+a^2Z_{b2}+aZ_{c2} \\ Z_{a1}+aZ_{b1}+a^2Z_{c1}+Z_{a2}+aZ_{b2}+a^2Z_{c2} & Z_{a1}+Z_{b1}+Z_{c1}+Z_{a2}+Z_{b2}+Z_{c2} \\ Z_{a1}+a^2Z_{b1}+aZ_{c1}+Z_{a2}+a^2Z_{b2}+aZ_{c2} & Z_{a1}+aZ_{b1}+a^2Z_{c1}+Z_{a2}+aZ_{b2}+a^2Z_{c2} \\ Z_{a1}+Z_{b1}+Z_{c1}-Z_{a2}-Z_{b2}-Z_{c2} & Z_{a1}+a^2Z_{b1}+aZ_{c1}-Z_{a2}-a^2Z_{b2}-aZ_{c2} \\ Z_{a1}+aZ_{b1}+a^2Z_{c1}-Z_{a2}-aZ_{b2}-a^2Z_{c2} & Z_{a1}+Z_{b1}+Z_{c1}-Z_{a2}-Z_{b2}-Z_{c2} \\ Z_{a1}+a^2Z_{b1}+aZ_{c1}+Z_{a2}+a^2Z_{b2}+aZ_{c2} & Z_{a1}+aZ_{b1}+a^2Z_{c1}-Z_{a2}-aZ_{b2}-a^2Z_{c2} \end{bmatrix} \cdots$$

$$\cdots\cdots \begin{bmatrix} Z_{a1}+aZ_{b1}+a^2Z_{c1}+Z_{a2}+aZ_{b2}+a^2Z_{c2} & Z_{a1}+Z_{b1}+Z_{c1}-Z_{a2}-Z_{b2}-Z_{c2} \\ Z_{a1}+a^2Z_{b1}+aZ_{c1}+Z_{a2}+a^2Z_{b2}+aZ_{c2} & Z_{a1}+aZ_{b1}+a^2Z_{c1}-Z_{a2}-aZ_{b2}-a^2Z_{c2} \\ Z_{a1}+Z_{b1}+Z_{c1}+Z_{a2}+Z_{b2}+Z_{c2} & Z_{a1}+a^2Z_{b1}+aZ_{c1}-Z_{a2}-a^2Z_{b2}-aZ_{c2} \\ Z_{a1}+aZ_{b1}+a^2Z_{c1}-Z_{a2}-aZ_{b2}-a^2Z_{c2} & Z_{a1}+Z_{b1}+Z_{c1}+Z_{a2}+Z_{b2}+Z_{c2} \\ Z_{a1}+a^2Z_{b1}+aZ_{c1}-Z_{a2}-a^2Z_{b2}-aZ_{c2} & Z_{a1}+aZ_{b1}+a^2Z_{c1}+Z_{a2}+aZ_{b2}+a^2Z_{c2} \\ Z_{a1}+Z_{b1}+Z_{c1}-Z_{a2}-Z_{b2}-Z_{c2} & Z_{a1}+a^2Z_{b1}+aZ_{c1}+Z_{a2}+a^2Z_{b2}+aZ_{c2} \end{bmatrix} \cdots$$

$$\cdots\cdots \begin{bmatrix} Z_{a1}+a^2Z_{b1}+aZ_{c1}-Z_{a2}-a^2Z_{b2}-aZ_{c2} & Z_{a1}+aZ_{b1}+a^2Z_{c1}-Z_{a2}-aZ_{b2}-a^2Z_{c2} \\ Z_{a1}+Z_{b1}+Z_{c1}-Z_{a2}-Z_{b2}-Z_{c2} & Z_{a1}+a^2Z_{b1}+aZ_{c1}-Z_{a2}-a^2Z_{b2}-aZ_{c2} \\ Z_{a1}+aZ_{b1}+a^2Z_{c1}-Z_{a2}-aZ_{b2}-a^2Z_{c2} & Z_{a1}+Z_{b1}+Z_{c1}-Z_{a2}-Z_{b2}-Z_{c2} \\ Z_{a1}+a^2Z_{b1}+aZ_{c1}+Z_{a2}+a^2Z_{b2}+aZ_{c2} & Z_{a1}+aZ_{b1}+a^2Z_{c1}+Z_{a2}+aZ_{b2}+a^2Z_{c2} \\ Z_{a1}+Z_{b1}+Z_{c1}+Z_{a2}+Z_{b2}+Z_{c2} & Z_{a1}+a^2Z_{b1}+aZ_{c1}+Z_{a2}+a^2Z_{b2}+aZ_{c2} \\ Z_{a1}+aZ_{b1}+a^2Z_{c1}+Z_{a2}+aZ_{b2}+a^2Z_{c2} & Z_{a1}+aZ_{b1}+a^2Z_{c1}+Z_{a2}+aZ_{b2}+a^2Z_{c2} \end{bmatrix}$$

$$a = e^{j120^\circ}.$$

is used to synchronize time. The six-sequence component transf-ormation is introduced, and with the help of the phase sequence selection rule, the nonlinear impedances of MOVs are eliminated. Simultaneously, to confirm the robustness of the algorithm, different fault types, different fault initial angles and different fault resistances are taken into account in the system simulation. Not only that, the influence of SCs installation positions, line parameter errors, different sampling rates and measurement errors are also tested. In general, the proposed fault location algorithm has excellent fault location performance.

APPENDIX

From Eq (20), $[Z_{SCs}]$ is shown at the top of the page given as follows:

REFERENCES

[1] M. KezunovicJ Mrkic and B. Perunicic, "An accurate fault location algorithm using synchronized sampling," *Electr. Power Syst. Res.*, vol. 29, no. 3, pp. 161–169, 1994, doi: 10.1016/0378-7796(94)90011-6.

[2] T. Lin, Z. Xu, F. B. Ouedraogo, and Y. Lee, "A new fault location technique for three-terminal transmission grids using unsynchronized sampling," *Int. J. Elect. Power Energy Syst.*, vol. 123, no. 12, pp. 123–135, 2020, doi: 10.1016/j.ijepes.2020.106229.

[3] B. Xia, Y. Wang, E. Vazquez, W. Xu, D. Wong, and M. Tong, "Estimation of fault resistance using fault record data," *IEEE Trans. Power Del.*, vol. 30, no. 1, pp. 153–160, Feb. 2015, doi: 10.1109/TPWRD.2014.2355041.

[4] Z. Moravej, O. Hajihosseini, and M. Pazoki, "Fault location in distribution systems with DG based on similarity of fault impedance," *TURKISH J. Electr. Eng. Comput. Sci.*, vol. 25, pp. 3854–3867, 2017, doi: 10.3906/elk-1606-461.

[5] X. Kong, Y. Xu, Z. Jiao, D. Dong, X. Yuan, and S. Li, "Fault location technology for power system based on information about the power Internet of things," *IEEE Trans. Ind. Informat.*, vol. 16, no. 10, pp. 6682–6692, Oct. 2020, doi: 10.1109/TII.2019.2960440.

[6] F. M. Aboshady, D. W. P. Thomas, and M. Sumner, "A new single end wideband impedance based fault location scheme for distribution systems," *Electr. Power Syst. Res.*, vol. 173, pp. 263–270, Aug. 2019, doi: 10.1016/j.epsr.2019.04.034.

[7] L. Bo Sheng and S. Elangovan, "A fault location method for parallel transmission lines," *Int. J. Elect. Power Energy Syst.*, vol. 21, no. 4, pp. 253–259, 1999, doi: 10.1016/S0142-0615(98)00043-X.

[8] G. Song, J. Suonan and Y. Ge, "An accurate fault location algorithm for parallel transmission lines using one-terminal data," *Int. J. Elect. Power Energy Syst.*, vol. 31, nos. 2–3, pp. 124–129, 2009, doi: 10.1016/j.ijepes.2008.10.001.

[9] N. Peng, L. Zhou, R. Liang, X. Xue, G. Piliposyan, and Y. Hu, "Fault location on double–circuit transmission lines by phase correction of fault recorder signals without accurate time synchronization," *Electr. Power Syst. Res.*, vol. 181, no. 16, pp. 125–141, 2020, doi: 10.1016/j.epsr.2020.106198.

[10] M. K. Mondal and S. Debnath, "Fault location in UPFC compensated double circuit transmission line using negative sequence current phasors," *Electr. Power Syst. Res.*, vol. 184, no. 13, pp. 265–270, 2020, doi: 10.1016/j.epsr.2020.106347.

[11] M. Nemati, M. Bigdeli and A. Ghorbani, "Impedance-based fault location algorithm for double-circuit transmission lines using single-end data," *J. Control, Automat. Elect. Syst.*, vol. 31, no. 5, pp. 1267–1277, 2020, doi: 10.1007/s40313-020-00620-w.

[12] B. Mahamedi and J. Guo Zhu, "Unsynchronized fault location based on the negative-sequence voltage magnitude for double-circuit transmission lines," *IEEE Trans. Power Del.*, vol. 29, no. 4, pp. 1901–1908, Aug. 2014, doi: 10.1109/TPWRD.2013.2294972.

[13] M. Coursol, C. T. Nguyen, R. Lord, and X.-D. Do, "Modeling MOV-protected series capacitors for short-circuit studies," *IEEE Trans. Power Del.*, vol. 8, no. 1, pp. 448–453, 1993, doi: 10.1109/61.180367.

[14] S. Qi, H. Zhao, and F. Qian, "Connection mode and protection of 500 kV transmission line series compensation capacitor bank," *Power Syst. Protection Control*, vol. 38, pp. 63–73, Jan. 2010.

[15] G. Manassero Junior, S. G. Di Santo, and D. G. Rojas, "Fault location in series-compensated transmission lines based on heuristic method," *Electr. Power Syst. Res.*, vol. 140, pp. 950–957, Nov. 2016, doi: 10.1016/j.epsr.2016.03.049.

[16] A. Capar and A. Basa Arsoy, "A performance oriented impedance based fault location algorithm for series compensated transmission lines," *Int. J. Elect. Power Energy Syst.*, vol. 71, no. 3, pp. 209–214, 2015, doi: 10.1016/j.ijepes.2015.02.020.

[17] M. M. Saha, E. Rosolowski, J. Izykowski, and P. Pierz, "Evaluation of relaying impedance algorithms for series-compensated line," *Electr. Power Syst. Res.*, vol. 138, pp. 106–112, Sep. 2016, doi: 10.1016/j.epsr.2016.03.046.

[18] A. Saffarian and M. Abasi, "Fault location in series capacitor compensated three-terminal transmission lines based on the analysis of voltage and current phasor equations and asynchronous data transfer," *Electr. Pow. Syst. Res.*, vol. 187, no. 7, pp. 414–428, 2020, doi: 10.1016/j.epsr.2020.106457.
[19] T. P. S. Bains, T. S. Sidhu, Z. Xu, I. Voloh, and M. R. D. Zadeh, "Impedance-based fault location algorithm for ground faults in Series-Capacitor-Compensated transmission lines," *IEEE Trans. Power Del.*, vol. 33, no. 1, pp. 189–199, Feb. 2018, doi: 10.1109/TPWRD.2017.2711358.
[20] R. Taheri, M. Eslami and Y. Damchi, "Single-end current-based algorithm for fault location in series capacitor compensated transmission lines," *Int. J. Elect. Power Energy Syst.*, vol. 123, no. 8, pp. 411–423, 2020, doi: 10.1016/j.ijepes.2020.106254.
[21] T. P. S. Bains and M. R. D. Zadeh, "Supplementary impedance-based fault-location algorithm for series-compensated lines," *IEEE Trans. Power Del.*, vol. 31, no. 1, pp. 334–342, Feb. 2016, doi: 10.1109/TPWRD.2015.2476341.
[22] Y. Zhang, J. Liang, Z. Yun, and X. Dong, "A new fault-location algorithm for series-compensated double-circuit transmission lines based on the distributed parameter model," *IEEE Trans. Power Del.*, vol. 32, no. 6, pp. 2398–2407, Dec. 2017, doi: 10.1109/TPWRD.2016.2626476.
[23] C. A. Apostolopoulos and G. N. Korres, "A novel fault-location algorithm for double-circuit transmission lines without utilizing line parameters," *IEEE Trans. Power Del.*, vol. 26, no. 3, pp. 1467–1478, Jul. 2011, doi: 10.1109/TPWRD.2010.2102777.
[24] C. A. Apostolopoulos and G. N. Korres, "Accurate fault location algorithm for double-circuit series compensated lines using a limited number of two-end synchronized measurements," *Int. J. Electr. Power Energy Syst.*, vol. 42, no. 1, pp. 495–507, Nov. 2012, doi: 10.1016/j.ijepes.2012.03.042.
[25] S. Nan, G. Yaozhong and T. Huiliang, "Six-sequence fault components and its characteristics on double-circuit line on the same pole," *Automat. Electr. Power Syst.*, vol. 5, no. 4, pp. 44–51, 1989.
[26] M. A. Jarrahi, H. Samet, and T. Ghanbari, "Fast current-only based fault detection method in transmission line," *IEEE Syst. J.*, vol. 13, no. 2, pp. 1725–1736, Jun. 2019, doi: 10.1109/JSYST.2018.2822549.
[27] A. T. Johns and S. Jamali, "Accurate fault location technique for power transmission lines," *IEE Proc. C Gener., Transmiss. Distrib.*, vol. 137, no. 6, pp. 395–402, Nov. 1990, doi: 10.1049/ip-c.1990.0054.
[28] C. Korasli, "Line-current compensated single toroidal-core current transformer for three-phase current measurement," *IEEE Trans. Power Del.*, vol. 22, no. 1, pp. 500–506, Jan. 2007.
[29] *IEEE Draft Standard for Series Capacitor Banks in Power Systems*, IEEE Standard P824/D1, Jul. 2019, vol. 4, no. 1, pp. 1–62.
[30] *IEEE Draft Standard for Synchrophasor Measurements for Power Systems*, IEEE Standard PC37.118.1/D4.2, May 2011, pp. 1–56.

DAIYING CAI received the bachelor's degree in electrical engineering and automation from the Chongqing University of Posts and Telecommunications (CQUPT), Chongqing, China, in 2018, where he is currently pursuing the master's degree. His research interests include power system analysis and transmission line fault location.

JUN ZHANG received the bachelor's degree in measurement and control technology from Chongqing Technology and Business University, in 2018. He is currently pursuing the master's degree with the Smart Energy Research Center, Chongqing University of Posts and Telecommunications. His research interests include intelligent obstacle avoidance and driverless technology.